ASIAN JOURNAL OF PHARMACEUTICAL AND CLINICAL RESEARCH

INNOVARE ACADEMIC SCIENCES
Knowledge to Innovation

Vol 18, Issue 8, 2025

Online - 2455-3891
Print - 0974-2441

Research Article

DESIGN OF EXPERIMENT-BASED CANDESARTAN CILEXETIL NANOCRYSTALS LOADED SOLID DISPERSION FOR ORAL DRUG DELIVERY SYSTEM: OPTIMIZATION, *IN VITRO/IN VIVO* EVALUATION

SONALI VIJAYKUMAR MAGDUM[1]*, PRAMODKUMAR JAYKUMAR SHIROTE[2]

[1]Department of Pharmaceutics, Dr. J. J. Magdum Pharmacy College, Jaysingpur, Maharashtra, India. [2]Department of Pharmaceutical Chemistry, Dr. Bapuji Salunkhe Institute of Pharmacy, Miraj, Maharashtra, India.
***Corresponding author: Sonali Vijaykumar Magdum; Email: svmagdum25@gmail.com**

Received: 16 April 2025, Revised and Accepted: 12 June 2025

ABSTRACT

Objective: The current study aimed to develop and characterize a nanocrystal-based solid dispersion of Candesartan Cilexetil (CC) to improve its solubility and bioavailability.

Methods: CC-loaded nanosuspension was prepared using the solvent precipitation method, employing Eudragit RLPO, and polyvinyl alcohol as a stabilizer. The resulting nano-sized lyophilized powder was then incorporated into a solid dispersion using the kneading method with crospovidone as a super-disintegrant. A 3^2 factorial design was used for optimization, with the amount of nanosuspension powder (X_1) and concentration of superdisintegrant agent (X_2) as independent variables. Evaluations included drug content (%), drug release (DR %), zeta potential (ZP), and other characterization techniques.

Results: The optimized formulation, CCSD9, exhibited a particle size of 264 nm, a ZP of 20.32 mV, a DR rate of 99.45%, and a polydispersity index (PDI) of 0.365. Transmission electron microscopy analysis revealed drug nanocrystal agglomeration, possibly due to the water removal process. Differential scanning calorimetry analysis indicated a minor change in crystallinity, likely due to lactose presence, and confirmed no significant drug-excipient interaction. A 6-month stability trial was conducted.

Conclusion: The solvent precipitation method proved to be an efficient approach for developing CC nanocrystal-based solid dispersion with a lower particle size. The nanosizing technique successfully encapsulated CC within the polymer matrix, enhancing DR and stability.

Keywords: Nanocrystal, Solid dispersion, Candesartan cilexetil, Eudragit RLPO, Oral bioavailability.

 DOI: http://dx.doi.org/10.22159/ajpcr.2025v18i8.54604. Journal homepage: https://innovareacademics.in/journals/index.php/ajpcr

INTRODUCTION

Candesartan Cilexetil (CC), known as an ester and prodrug of parent candesartan (C), is designed to enhance the material's lip, hence improving penetration and absorption. CC has a limited and inconsistent amount of drug absorption, ranging from 15% to 40%, with literature reviews showing variations and contradictions about its value as an antihypertensive medication [1]. Some researchers give CC low, and Candesartan has an uncertain bioavailability due to its high fluidity and low affinity for water, while some believe it is related to premature disintegration by esterase activity organisms in the intestines before absorption, generating the weakly bioavailable positive molecule [2].

The gastrointestinal esterase enzymes dissolve the ester bond of CC, making it active, and producing the active compound Candesartan, which is responsible for its antihypertensive effect. Following oral administration, CC itself was not detected in plasma; only metabolite Candesartan was observed [3]. According to research, the rate of production of the active portion in ester products is unknown and varies depending on the availability of esterase catalysts in the body, as well as variances in Enzyme diversity, which causes toxicological and dangerous differences. Few studies have been carried out to improve the efficacy of CC, employing typical procedures such as complex incorporation of CC with β-cyclodextrin, liquisolid tablets, and solid dispersions, or advanced nano drug delivery systems involving solid lipid nanoparticles, nanoemulsions, self-emulsifying drug delivery systems, niosomes, and nanocrystals [4-6].

CC, a BSC class II drug that has poor solubility but good permeability, and is determined in alkaline surroundings above its pKa, could be a useful technique to improve its solubility and bioavailability. Recent studies have shown that incorporating Tris with challenging drugs can significantly enhance dissolution rates, bioavailability, solubility, stability, and membrane permeability. In metabolic acidosis treatment, tris is a synthetic amino acid addition that functions as a stabilizing and alkalinizing substance. Has been shown to increase esterase activity, reduce bioavailability variability, and reduce changes in the Cleavage of ester linkages during prodrug activation. The choice of an appropriate carrier is critical for developing an effective solid dispersion formulation, as the carrier's qualities have a substantial impact on drug-dissolving characteristics. Research shows that adding acidifiers or alkalinizers to solid dispersion formulations of weakly acidic or fundamental pharmaceuticals with low water solubility can increase dissolution rates by moderating the pH of the microclimate in the dispersion zone. For instance, studies have demonstrated that the solid dispersion of telmisartan with PEG 6000, combined with various alkalinizers, resulted in a notable improvement in dissolution rates and, consequently, enhanced bioavailability [5-10].

The goal of this work was to enhance the effectiveness of CC, a strong and targeted cardiovascular medication with a fluctuating and limited bioavailability, by creating nanocrystals by a simple solid dispersion method effectiveness of CC, a strong and targeted cardiovascular medication with a fluctuating and limited bioavailability, by creating nanocrystals by a simple solid dispersion method. This approach involved utilizing tromethamine, an alkaline esterase activator carrier,

to address the controversial effects of esterase enzymes and improve the drug's performance.

MATERIALS AND METHODS

Materials

Dr. Reddy's Laboratories, Hyderabad, generously provided the CC. We purchased Eudragit (RLPO) from Evonik Lab in Mumbai. While methanol (High-performance liquid chromatography [HPLC] grade) was acquired from LOBA Chemie Pvt. Ltd., sodium starch glycolate and lactose they bought from Sigma Aldrich Ltd., Mumbai. The remaining compounds were all pure analytical grade.

Instruments

The following instruments were used in the study: an electronic balance (SR Electronics, Mumbai, India), magnetic stirrer (Remi Equipment Ltd., Mumbai, India), high-pressure homogenizer (Panda PLUS 1000, GEA NiroSoavi, USA), fourier transform infrared (FTIR) spectrophotometer (BRUKER ALPHA, Germany), particle size analyzer (Nanoparticle analyser SZ-100, Horiba Scientific, Japan), ultraviolet (UV)/Visible spectrophotometer (Shimadzu 1800, Japan), dissolution apparatus (Lab India DS 8000, Mumbai, India), ultrasonicator (Ultrasonic Processor VC505, Sonics and Materials Inc., USA), X-ray diffraction (XRD) (Xpert MPD, Philips, Holland), cooling centrifuge (Remi C30 PLUS, Mumbai, India), pH meter (Digital Systronic, Mumbai, India), scanning electron microscope (Nova SEM-450, USA), and HPLC (Shimadzu LC-20 AD).

Methods

Preparation of nanosuspension by the solvent evaporation method

Screened solvents like acetone and methanol were used in the solvent evaporation approach for the nano-precipitation method. The loading of CC into the nanosuspension was done. Numerous polymers and surfactants, such as polyvinyl alcohol (PVA) and Eudragit (RLPO), were assessed as stabilizers, both singly and in combination. By optimizing processing dimensions and attributes, such as stabilizer type, drug-to-surfactant ratio, solvent-to-antisolvent ratio, and rotating speed, the desired zeta potential (ZP) and particle size were reached. Sonication was performed utilizing an Ultrasonic Processor VC505 from Sonics and Materials Inc., USA, after nanoprecipitation in the combined procedure incorporating probe sonication. Five minutes of a 5-s on, 3-s-off, 25% amplitude pulses were used during the sonication [11]. In the combination approach utilizing High-Pressure Homogenization (HPH), a suspension was prepared using the same nanoprecipitation technique, and then HPH was applied using a Panda PLUS 1000 from GEA NiroSoavi, USA. After five cycles at 500 bars, the homogenization was carried out for fifteen cycles at 800 bars. Each batch was prepared in triplicate (n=3).

Lyophilization of CC-loaded nanosuspension

A Christ Alpha 4D Plus lyophilized from the USA was used to lyophilize an optimum batch to guarantee the stability of the nanosuspension. Although particular data is not provided here in the same detail as in previous sections, a variety of cryoprotectants were assessed for their compatibility with the medication.

Two possible cryoprotectants that were examined were lactose and sodium starch glycolate. Initially, a 10% concentration of these cryoprotectants was introduced. After 48 h of freezing at −80°C and thawing at ambient temperature, the nanosuspension underwent two cycles of freezing and thawing. Particle size and PDI measurements were made after thawing.

Samples were first frozen at −45°C for lyophilization, and then they were dried both primary and secondary. Primary drying was started at −30°C and 250 mT of pressure. There were sporadic holds at −25°C for different lengths of time. Subsequent drying was carried out at 10°C for 300 min at 150 mT of pressure after the initial drying process [12,13].

Characterization of CC loaded nanosuspension

Particle size, polydispersity index (PDI), and ZP

A Vesicle sizer (HORIBA) utilizing dynamic light scattering was employed to determine the PDI and the average particle size. With the same apparatus, ZP testing was also carried out. 1 mg of the lyophilized product was once more disposed of in 3 mL of Milli-Q water for analysis. To make sure the sample was spread evenly, vertexing was done as needed. Three measurements were taken for each [14].

FTIR study

With the aid of a BRUKER Alpha II FTIR Spectrophotometer, FTIR spectra were acquired for a variety of materials, including pure medication, excipients, physical mixes, and the improved formulation. After each sample, weighing around 5 mg, its spectra were collected between 400 and 4000 cm^{-1} [15].

Differential scanning calorimetry (DSC) study

The refined formulation, physical mixes, excipients, and pure pharmaceuticals were all subjected to DSC analysis utilizing a Shimadzu DSC-50 device that is based in Kyoto, Japan. Each sample was carefully weighed out to a volume of 40 mL in standard aluminum crucible pans. The lids were sealed with small holes, and the formulation was warmed from 0°C to 360°C at a rate of 40°C/min. To prepare for the analysis, the crucibles were secured to a steel platform using double-sided adhesive tape [16].

XRD study

To assess the sample's physical condition, XRD was utilized. Cu/Ni radiation was used in an XRD instrument (Xpert MPD, Philips, Holland) to document the drug's unprocessed XRD patterns, the drug's lyophilized form without cryoprotectant, and the lyophilized nanosuspension. A scan rate of 2°/min was applied to the diffractograms, covering a range of 0°–50° 2θ. Sample holders were filled with crushed samples that had been ground with a mortar and pestle before analysis [17].

Determination of encapsulation efficiency

Three hours at 10,000 rpm and 7°C were spent centrifuging the formulation using a cooling centrifuge (24 BL model, Remi, Mumbai, India). A UV/visible spectrophotometer (Shimadzu 1800, Japan) was utilized to determine the absorbance of the drug concentration at 257 nm after separating the supernatant. The entrapment efficiency (EE) of CC was calculated by subtracting the amount of free drug from the initial amount of drug administered [15,18]. The %EE for each formulation was calculated with the help of the following formula:

$$EE\ (\%) = \text{Initial drug} - \text{final drug} / \text{Initial drug} \times 100$$

Stability studies

To conduct stability experiments for the nanosuspension, the formulation was stored at 4°C, with samples collected on days 0, 30, 60, and 90. Vesicle size, ZP, and EE of each sample are measured using the Zetasizer (HORIBA) and the previously described method. Three duplicates of each study were conducted [19].

Fabrication of CC nanosuspension solid dispersion by kneading method

Hydroxypropyl β-cyclodextrin or PVP K30, the carrier, and the necessary quantities of lyophilized powder were mixed in ratios of 1:1, 1:1.5, and 1:2. Using a glass mortar, this mixture was thoroughly kneaded for 30 min after being moistened with an acceptable amount of methanol. The final homogenous paste was allowed to dry in a hot air oven at 40°C for 24 h. The compound became dry and powdered into tiny particles. Put through a 60-mesh screen and kept in an airtight container [20].

Experimental design

To optimize the formulation of the produced batches, we used an FFD with DES, Trial version 11.0. Throughout nine experimental runs, this strategy allowed for a methodical assessment of the effects

of different formulation parameters. Drug content (Y1), *in vitro* drug release (DR) (Y2), and ZP (Y3) were considered dependent factors in this investigation, whereas the concentrations of disintegrant (X_2) and nanosuspension powder (X_1) were selected as independent variables. This investigation aimed to determine how these answers vary about the two chosen factors. Table 1 indicates 3^2 Factorial designs for Formulation Batches. Table 2 shows coded and actual values.

Generation of polynomial equations

We used the Response Surface Methodology with the Design software, Tri. Ver. 11.0 to carry out a number of simulations in our present optimization project. We created polynomial models with interactions for each response variable by applying the MLRA approach.

Statistical analysis of data

We employed statistical analytic techniques, notably analysis of variance (ANOVA) with DES (ver. 11.0), to evaluate the impact of external influences on the replies. To determine statistical significance, a cutoff of $p<0.05$ was set.

Generation of 3D response surface plots

We created three-dimensional plots that show variations in the response surface to visually represent the measured responses. By showing how independent variables affect results graphically, these plots help analyse the simultaneous impacts of two factors on a response [7].

Characterization of prepared solid dispersion

Phase solubility study

Different concentrations of aqueous PVP-K30 solutions (0.2–2%) in double-distilled water were placed in a succession of stoppered conical flasks, and levels of candesartan (C) were added until the solution reached a maximum of solubility. Once equilibrium was reached, the samples were mixed with water twice distilled, and the pharmaceutical concentration was determined using a UV-visible spectrophotometer (Shimadzu-1601, Shimadzu Corp, Japan) set to a wavelength of 255 nm. PVP-K30 at an equivalent concentration in double-distilled water was used as a blank for the measurements. Three replications at room temperature were performed for each experiment [21].

Table 1: 3^2 Factorial design for formulation batches

Formulation code	Independent variables			
	X_1	X_2	X_1	X_2
CCSD-1	−1	−1	75	3
CCSD-2	−1	0	75	5
CCSD-3	−1	+1	75	7
CCSD-4	0	−1	100	3
CCSD-5	0	0	100	5
CCSD-6	0	+1	100	7
CCSD-7	+1	−1	125	3
CCSD-8	+1	0	125	5
CCSD-9	+1	+1	125	7

1: Minimum value, 0: Middle value, +1: Maximum value

Table 2: Coded and actual values

Independent Variables	Levels		
	Low (−1)	Medium (0)	High (+1)
Concentrations of nanocrystals (X_1)	75 mg	100 mg	125 mg
Concentration cross-povidone (X_2)	3 mg	5 mg	7 mg
Dependent variables	Y1	Drug content	
	Y2	*In vitro* drug release	
	Y3	Zeta potential	

Drug content

Solid dispersions and physical mixes of CC and PVP-K30 (10 mg CC in 10 mL of methanol) have been generated and then filtered through a 0.45 μm filter. After suitable dilution with phosphate buffer (pH 7.4), which served as the blank, the samples were analyzed using a UV-visible spectrophotometer to measure the drug concentration at 255 nm. Three runs of each experiment were conducted [22].

Dissolution study

Dissolution tests were carried out utilizing a USP Type II Paddle dissolving equipment (DS-6000, LABINDIA, India). The system was made up of 900 mL of pH 7.4 phosphate buffer, which was maintained at 37±0.5°C and agitated at 50 rpm, and was combined with 10 g of glass beads and 10 mg of solid dispersion (CC) samples. This was done to prevent powder agglomeration in the dissolution medium. Samples were obtained every 5, 10, 15, 30, 45, and 60 min. They were subsequently reinstated with fresh dissolving medium after being filtered via 0.45 μm filter paper. A spectrophotometric analysis was utilized to measure the quantities at 255 nm. Three different DR assays were performed [23].

DR kinetics study

Using a range of kinetic equations, including zero-order release kinetics, first-order release kinetics, and the Higuchi model, we fully examined the DR kinetics from the solid dispersion powder.

Consequently, based on our analysis of the release data, several important metrics were produced. "n" and "k" denoted the time component and release rate constant, respectively. We also computed the regression coefficient, or "R," using the Korsemeyer–Peppas equation, which provided crucial information on the release procedure.

We used different models to analyze the available DR profile and better understand the underlying mechanisms of DR. The models included zero-order, first-order, Higuchi, Hixson–Crowell, and Korsemeyer–Peppas. We were able to evaluate the regression values' (R^2) goodness of fit, and determine which model best captured the release behavior thanks to this thorough technique [24].

Transmission electron microscopy (TEM)

The morphology of solid dispersion powder loaded with CC was examined using TEM. The lamellarity dimension and geometry of the solid dispersion structure are investigated by TEM imaging. An accelerated voltage of 120 kV was used to evaluate the samples [25].

***In vivo* pharmacokinetics study of CC-loaded solid dispersion**

Protocol of experiments

Using the guidelines of the Association with Research, animal study was conducted to evaluate pharmacokinetic parameters such as C_{max}, T_{max}, and area under the curve (AUC) for different solid dispersion formulations. Total number of animal procedures granted by the IAEC board of Biocyte Institute of Research and Development, Plot No. 20, Shriram Residency, Kalanagar, Sangli (M.S.) 416416 in Sangli, Maharashtra (Proto. no. IAEC/Sangli/2022-23/10).

Following a fast lasting 12 h, all rats are separated into 3 sets of 9 each. The rats, weighing between 0.25 and 0.30 kg, are kept in a prescribed facility with a 12-h light-dark cycle and daily temperature of 22°C/30°C. They have free access to water and normal food. The free CC suspension is equivalent to 8 mg/kg of CC and is distributed in a 0.5% sodium carboxymethyl cellulose solution (1.0 mg/kg). The retro-orbital vein was used to draw serial blood samples (0.3 mL) at 0.5, 1, 2, 4, 6, 8, 10, 12, and 24 h after injection [26,27].

The three groups were administered the following treatments:

1. The first set of animals acquired 8 mg/kg of the optimized formulation of CC

2. The second set of animals acquired 8 mg/kg of the marketed formulation of CC
3. The third set of animals acquired 8 mg/kg of a plain nanosuspension of CC.

Blood processing

Next, 200 µL of blood was collected from the femoral artery at specified intervals up to 24 h after the injection. The samples were mixed with heparin to prevent blood coagulation. They were then rotated at 5000 rpm for 5–10 min to separate the plasma, and they were subsequently stored at −20°C.

Chromatographic analysis using HPLC

Chromatographic separation of CC was performed using an ACN-5 mM sodium (80:20, v/v) mobile phase, pH adjusted to 3.5 using CH3COOH, and a flow rate of 0.8 mL/min.

The extraction was performed on a Waters Reliant C18 column (250 mm × 4.6 mm, 5 µm) covered by a precolumn guard cartridge. The sample was detected at 256 nm. A temperature of 30°C was maintained for the chromatographic phase.

RESULTS AND DISCUSSION

The solid dispersion of CC significantly enhanced the dissolution rate, which is a critical factor for improving the oral bioavailability of poorly water-soluble drugs. By reducing particle size to the nanocrystal range and embedding the drug within a hydrophilic polymer matrix, the system ensures rapid disintegration and efficient DR. This approach facilitates faster absorption in the gastrointestinal tract, making it a promising strategy for effective and consistent drug delivery in clinical applications.

Data optimization of 3^2 full factorial design

Quadratic equations

The quadratic equation for the response is as follows:

$$Y=\beta0+\beta1\ A+\beta2\ B+\beta3\ AB+\beta4\ A2+\beta5\ B2$$

In the above equations, where Y is an independent variable, 0 is an average outcome from nine batches, and 1 is an estimated coefficient for factor A, the impacts of factors A and B reflect that the total response of each factor is individually varied across lower and higher ratios. However, the correlated terms (AB) demonstrate how changing both factors at once changes the outcome. ZP (X_3), *in vitro* DR (X_2), and drug content (X_1) are all highly influenced by the independent parameters selected, according to an examination of the Design of Experiments data. Using the mathematical signs contained in the given polynomial equations, inferences can be made. An indication of synergy is favorable.

Where factors work together, conversely, a negative sign denotes an antagonistic impact in which variables oppose one another [24].

$$Y1–(DC)=87.11+1.88\ A+4.67\ B+1.11\ AB-0.52\ A^2+1.47\ B^2$$

$$Y2–(DR)=90.42+0.54\ A+1.09\ B-0.65\ AB-0.25\ A^2-2.42\ B^2$$

$$Y3–(ZP)=12.88+1.12\ A+3.50\ B+0.66\ AB+0.76\ A^2+0.28\ B^2$$

Where

- A=Amount of nanosuspension powder
- B=Amount of disintegrant

The factorial design data of CC nanocrystal-based solid dispersion are presented in Table 3.

Statistical analysis

All results are analyzed using sophisticated software (Design-Expert, version 11.0). It was clear using the results that all of the dependent variables had p-values lower than 0.05 ($p<0.05$). It was discovered that the ZP, DR, and DC models F had values of 12.88, 90.42, and 87.11, respectively. It highlights how important the model is. R-squared is a statistical measure of the degree to which the data agree with the fitted regression curve. In several regression instances, it is also known as the coefficient of prediction. In linear regression models, the goodness-of-fit measure known as R-squared is employed. The dependent variable's proportion of variance by the independent factors taken together is displayed [28]. Table 4 shows ANOVA for the Quadratic models of content (Y1). Table 5 indicates ANOVA for quadratic models, indicating the model F-value of Drug content (Y1). Table 6 shows ANOVA for Quadratic models of DR (Y2). Table 7 presents ANOVA for quadratic models, indicating the model F-value of DR. Table 8 shows ANOVA for Quadratic models of ZP (Y3). Table 9 presents ANOVA for quadratic models, indicating the model F-value of ZP.

Counter plots exhibiting the effect of varying amounts of nanosuspension powder and disintegrant

Three-dimensional graphs are made to measure the shift in the response surface for the measured responses. Based on the foregoing data on nanosuspension powder and disintegrant, it was determined that with an increase in concentration, powder created with increased drug absorption occurred (Fig. 1a). Based on the foregoing data on nanosuspension powder and disintegrant, it was determined that with a rise in concentration, greater drug release was possible from the

Table 3: Factorial Design data of Candesartan Cilexetil nanocrystal-based solid dispersion

S. No.	Formulation code	Drug content in % (Y1)	DR (at 60 Min) % (Y2)	Zeta potential mV (Y3)
1	CCSD-1	81.12±0.64	82.46	16.8
2	CCSD-2	84.77±0.82	90.84	17.89
3	CCSD-3	87.78±1.22	93.16	16.89
4	CCSD-4	89.77±1.48	95.42	17.89
5	CCSD-5	91.10±1.62	95.33	14.56
6	CCSD-6	92.10±1.18	96.00	20.45
7	CCSD-7	95.33±1.88	97.17	18.80
8	CCSD-8	97.01±0.92	98.00	19.75
9	CCSD-9	98.91±1.66	99.45	21.40

All values are expressed as mean±standard deviation, n=3

Table 4: Analysis of variance for Quadratic models of content (Y1)

Source	Coefficient estimate	Df	Standard error	95% Cl	95% CL	VIF
Intercept	87.11	1	0.75	84.73	89.49	
A-Amt. of Nanosuspensioned Powder	1.88	1	0.41	0.58	3.19	1.00
B-Amt. of Disintegrant	4.87	1	0.41	3.57	6.17	1.00
A^2	1.11	1	0.50	−0.48	2.70	1.00
B^2	−0.52	1	0.71	−2.77	1.74	1.00
AB	1.47	1	0.71	−0.78	3.73	1.00

Df: Degree of freedom, F-value: Ratio of two variation, p-value: Probability value, CL: Confidence level

Table 5: Analysis of variance for quadratic models indicating model F-value of Drug content (Y1)

Std. Dev.	1.00	R^2	0.9829
Mean	87.55	Adjusted R^2	0.9545
C. V.%	1.14	Predicted R^2	0.7993
Press	35.41	Adeq. Precision	16.508

Std. Dev.: Standard deviation, C.V: Coefficient of variance, R^2: Coefficient of determination, Adeq. Precision: Adequate precision. All values are expressed as mean±standard deviation, n=3

Table 6: Analysis of variance for Quadratic models of drug release (Y2)

Source	Coefficient estimate	Df	Standard Error	95% CL	95% CL	VIF
Intercept	90.42	1	0.30	89.47	91.36	
A-Amt. of Nanosuspensioned Powder	0.54	1	0.16	0.030	1.06	1.00
B-Amt. of Disintegrant	3.12	1	0.16	5.88	6.91	1.00
A^2	−0.65	1	0.20	−1.29	−0.024	1.00
B^2	−0.25	1	0.28	−1.14	0.64	1.00
AB	2.42	1	0.28	1.53	3.31	1.00

Df: Degree of freedom, F-value: Ratio of two variations, p-value: Probability value, CL: Confidence level

Table 7: Analysis of variance for quadratic models indicating model F-value of Drug release

Std. Dev.	0.40	R^2	0.9982
Mean	91.86	Adjusted R^2	0.9952
C. V. %	0.43	Predicted R^2	0.9793
Press	5.39	Adeq. Precision	43.949

Std. Dev.: Standard Deviation, C.V: Coefficient of variance, R^2: Coefficient of determination, Adeq. Precision: Adequate precision

Table 8: Analysis of variance for quadratic models of zeta potential (Y3)

Source	Coefficient estimate	Df	Standard Error	95% CL	95% CL	VIF
Intercept	12.88	1	0.39	11.65	14.11	
A-Amt. of Nanosuspensioned Powder	1.12	1	0.21	0.44	1.79	1.00
B-Amt. of Disintegrant	3.50	1	0.21	2.83	4.18	1.00
A^2	0.66	1	0.26	−0.17	1.49	1.00
B^2	0.76	1	0.37	−0.41	1.94	1.00
AB	0.28	1	0.37	−0.89	1.45	1.00

Df: Degree of freedom, F-value: Ratio of two variations, *P* value: Probability value, CL: Confidence level

Table 9: Analysis of variance for quadratic models indicating model F-value of Zeta Potential

Std. Dev.	0.52	R^2	0.9904
Mean	13.58	Adjusted R^2	0.9745
C. V. %	3.83	Predicted R^2	0.9089
Press	7.74	Adeq Precision	22.470

Std. Dev.: Standard deviation, C.V: Coefficient of variance, R^2: Coefficient of determination, Adeq. Precision: Adequate precision

created powder (Fig. 1b). Particle size may vary depending on the conc, and the disintegrant is crucial to the creation of nanosuspension powder. ZP increases as the concentration of super disintegrants increases, according to the response surface plots. Consequently, the ZP falls when the nanosuspension powder concentration rises (Fig. 1c) [29].

Particle size, PDI, and ZP

Prepared batches of particle sizes varied from 203 nm to 264 nm. The biggest particle size was detected by the CCNS-9, while the smallest was detected by the CCNS-1 among the equipment employed. Particle size and processing variables, including polymer and surfactant content, were found to be correlated. With median particle sizes (<260 nm), the CCNS-3, CCNS-4, CCNS-5, CCNS-6, and CCNS-8 batches stood out as being appropriate for oral administration. Furthermore, as illustrated in Table 9, there was a direct correlation between average particle size and polymer content in the CCNS formulations, with smaller particle sizes resulting from greater polymer concentrations [30]. When evaluating the degree of stability and electrical charge of nanoparticulate systems, ZP is an important consideration. Higher values of ZP, whether favorable or adverse, generally enhance stability by promoting electrostatic repulsion between particles with similar charges, thus preventing aggregation. The ZP values for CC nanocrystals are presented in Table 10. The optimized formulation demonstrated a ZP of around 20.32, indicating improved stability. This stability is influenced by variations in polymer and surfactant concentrations [29].

Compatibility study by FTIR

The FTIR was performed to confirm the likelihood of a chemical bond interaction between the medicine and the formulation's excipients. In Fig. 2, the combined infrared spectra of the formulation, drug, and polymer in physical combinations, polymer and drug, and pure drug were displayed. Asymmetric C-O-C stretching at 1074.31 cm^{-1}, an asymmetric C-O-C stretching at 1751.88 cm^{-1}, C-O stretching with in-plane bending at 1031.89 cm^{-1}, C=O stretching at 1751.88 cm^{-1}, and C-H out-of-plane bending at 745.50 cm^{-1} are some of the prominent peaks visible in the purified CC FTIR spectrum [30]. The FTIR spectrum of Eudragit RLPO exhibited a prominent peak at 3432 cm^{-1}. A tertiary amine was identified at 1731 cm^{-1} with an intensity of 1 cm^{-1}. In addition, characteristic peaks were observed at 1450.2 cm^{-1} corresponding to $-CH_3$ bending vibrations and at 4 cm^{-1} attributed to the C=O (ester) functional group. Key peaks in the drug-polymer physical combination were discovered in 1728. For C=O (ester), 1174, 6 cm^{-1}. For C–O stretching, 8 cm^{-1}, 1604.The values for C=C (aromatic stretching) are 1 cm^{-1}, –CH3 bending is 1453.1 cm^{-1}, the carboxyl group is 1728.6 cm^{-1}, and 2960. For O–H (carboxylic acid), 9 cm^{-1} [31]. According to the formulation's spectrum, there are distinctive peaks at 3029. O-H axial deformation, which peaked at 2031, was the cause of the 62 cm^{-1} and 65 cm^{-1} because of the C=O stretching (ketone), which peaks at 1423. Triazole or N=N=N stretching, was the cause of the 65 cm^{-1} peak at 1485.28 cm^{-1} due to the presence of Triazole N=N=N stretching was responsible for the peak at 1485.28 cm^{-1} caused by C-H bending vibration, whereas the peak at 1099.63 cm^{-1} was caused by the presence of C-O stretching primary alcohol [29]. Fig. 2 shows the FTIR

Table 10: Physicochemical characterization of CC-loaded nanosuspension

S. No.	Formulation batches	Particle size (nm)	Polydispersity index	Zeta potential (mv)	Encapsulation efficiency (%)
1.	CCNS-1	203	0.698	13.01	19.23±2.11
2.	CCNS-2	209	0.321	16.87	38.20±7.32
3.	CCNS-3	211	0.546	19.32	42.32±2.96
4.	CCNS-4	221	0.214	12.88	51.36±8.95
5.	CCNS-5	234	0.587	13.65	65.78±1.96
6.	CCNS-6	239	0.369	14.21	72.65±8.78
7.	CCNS-7	243	0.215	18.14	82.65±9.63
8.	CCNS-8	252	0.365	19.63	89.65±4.74
9.	CCNS-9	264	0.365	20.32	92.69±4.87

CCNS: Candesartan cilexetil-loaded nanosuspension, nm: Nanometer, mv: Millivolts, CC: Candesartan cilexetil, All values are expressed as mean±standard deviation, n=3

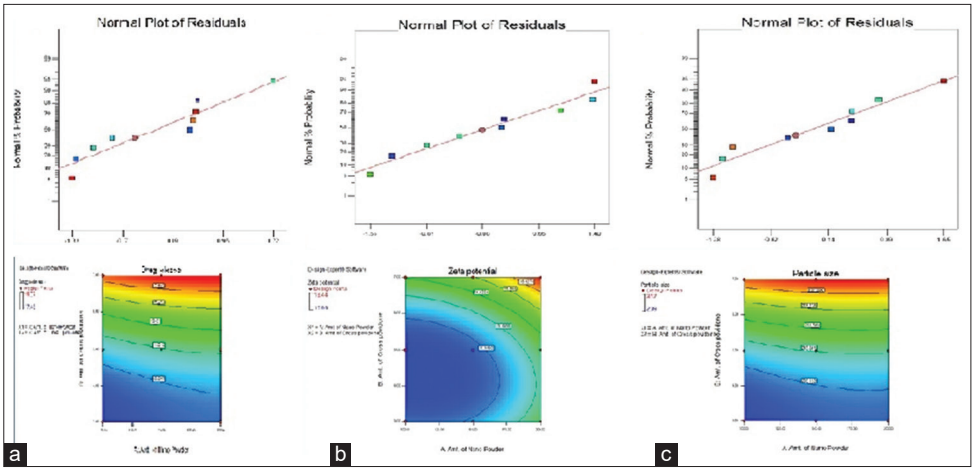

Fig. 1: Counter plots and 3D responses of (a) Drug content, (b) *In vitro* drug release, (c) Zeta potential

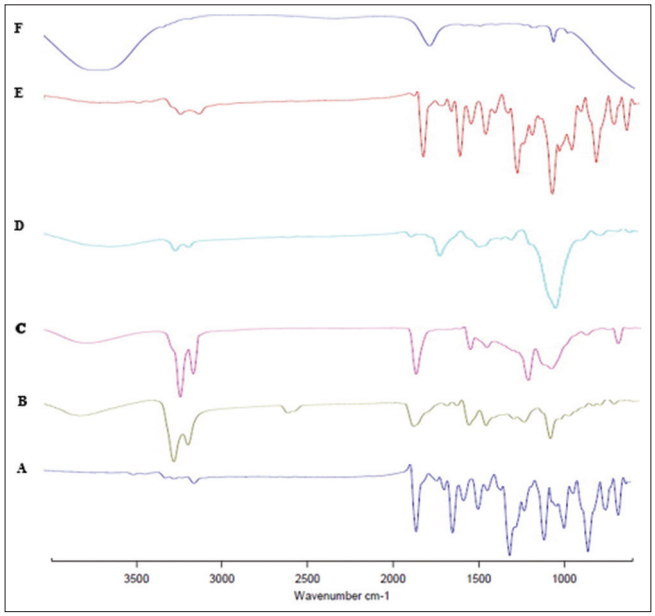

Fig. 2: Fourier transform infrared layout of (A) Candesartan cilexetil, (B) Eudragit RLPO (C) Polyvinyl alcohol (D) Lactose (E) Physical mixture (F) Formulation (CCNS-9)

layout of (A) CC, (B) Eudragit RLPO (C) PVA (D) Lactose (E) Physical mixture (F) and Formulation (CCNS-9).

DSC

The properties of melting and recrystallization of different substances are investigated using DSC. The CCNS-9 formulation, Lactose, PVA, Eudragit RLPO, CC, and DSC thermograms were examined. A notable endothermic peak at 171.91°C was seen in CC, suggesting that it is a crystalline substance. Melting endotherms were visible for Eudragit RLPO at approximately 268.85°C and for PVA at 200°C and 198.3°C. The physical mixture's thermal curve showed distinct melting point endotherms at 137.02°C, 138.32°C, and 224.89°C. Furthermore, a peak at 149.68°C was presented by the CCNS-9 formulation. The medicine and other ingredients in the formulation do not appear to interact significantly, according to these results [32,33]. Fig. 3 shows the DSC layout of (A) CC, (B) Eudragit RLPO (C) PVA (D) Lactose (E) Physical mixture (F) Formulation (CCNS-9).

XRD study

The drug's distinctive peaks at 2θ values of 172.29, 122.12, 19.8, 21.6, and 26.08 were found by XRD examination, confirming its crystalline shape. As seen in Fig. 4, however, upon lyophilization, the intensity of these

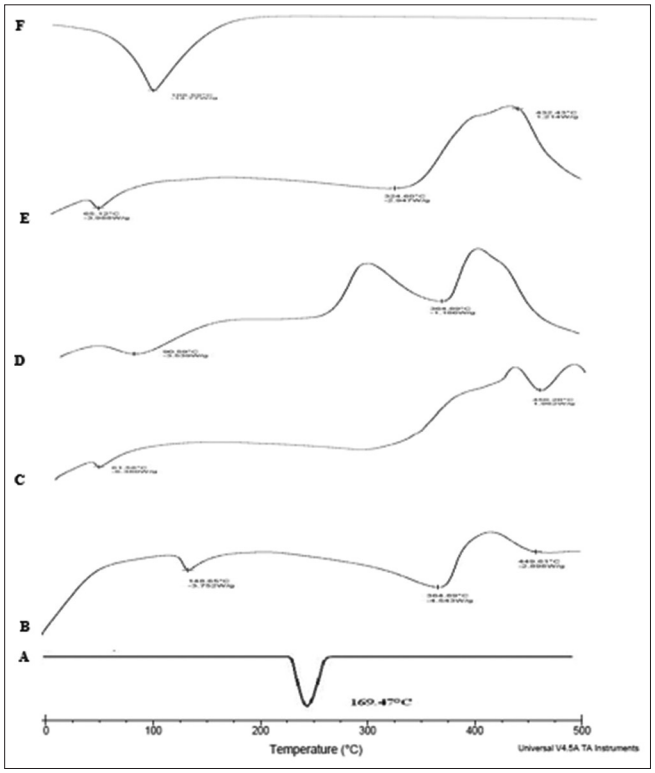

Fig. 3: Differential scanning calorimetry layout of (A) Candesartan cilexetil, (B) Eudragit RLPO (C) Polyvinyl alcohol (D) Lactose (E) Physical mixture (F) Formulation (CCNS-9)

peaks dramatically dropped, suggesting that the medication had partially amorphized in the lyophilized sample [34]. Several researchers have noted this post-lyophilization amorphization or partial amorphization of the active component. The stress created by the freeze-drying procedure, which entails the crystallization and sublimation of water, is most likely what caused this transition. Certain solutes have structural alterations that result in amorphization during the cooling phase when the solution hardens [35]. Fig. 4 shows the XRD layout of (A) CC, (B) Eudragit RLPO (C) PVA (D) Lactose (E) Physical mixture (F) Formulation (CCNS-9)

Determination of encapsulation efficiency

Table 10 illustrates that with a larger ratio of polymer to drug, the drug encapsulation efficiency rose from 19.23±2.11% to 92.69±1.98%. Regarding encapsulation efficiency, CCNS-9 outperformed the other formulations ($p<0.05$) [36].

Stability studies

For 3 months, the drug nanosuspension did not change much in size at 4°C. Minimal increases in size and polydispersity index (PDI) were seen when sampling at different intervals. Nanosuspensions are frequently unstable due to Ostwald ripening, a phenomenon where larger crystallites grow at the expense of smaller ones. Physical instability is generally associated with a rise in size and PDI, which causes nanosuspension development into the micron range and sample non-homogeneity. The nanosystems exhibited physical stability under storage conditions, with only slight increases observed in particle size and PDI, as presented in Table 11 [37].

Owing to the faster storage conditions, stability tests at 25°C showed a somewhat bigger rise in particle size compared to samples kept at 4°C. The larger kinetic energy at higher temperatures, which raises collision frequency and increases the likelihood of aggregation, is most likely the cause [38]. Table 11 presents the Stability study of the optimized batch of nanocrystal formulation (CCNS-9).

Phase solubility study

Fig. 5 displays the phase solubility studies with CC by using the PVP-K30. 159.8 M^{-1} was found to be the apparent stability constant (Ks). When the polymer concentrations in water increased from 0.1 to 2 µg/mL, the drug's solubility (r^2>0.6) increased linearly, indicating an AL-type solubility curve. The findings, which are displayed in Table 12, demonstrate that spontaneous solubilization was confirmed at all PVP-K30 doses (0.1–2 µg/mL) because the Gibbs free energy change (ΔG°tr) values are negative [36]. Table 12 shows the Gibbs-free energy of transfer for the solubilization process of CC in aqueous solutions of PVP K −30 at 37°C and Fig. 5 shows the phase solubility analysis plot.

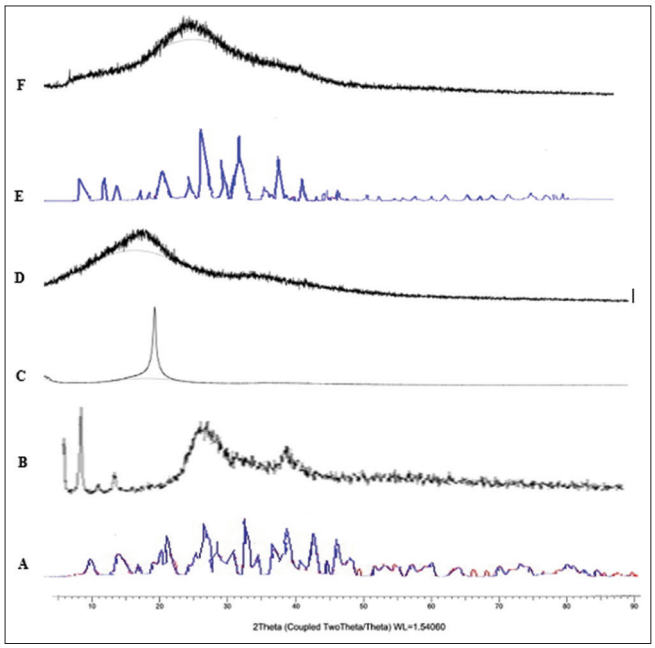

Fig. 4: X-ray diffraction layout of (A) Candesartan cilexetil, (B) Eudragit RLPO (C) Polyvinyl alcohol (D) Lactose (E) Physical mixture (F) Formulation (CCNS-9)

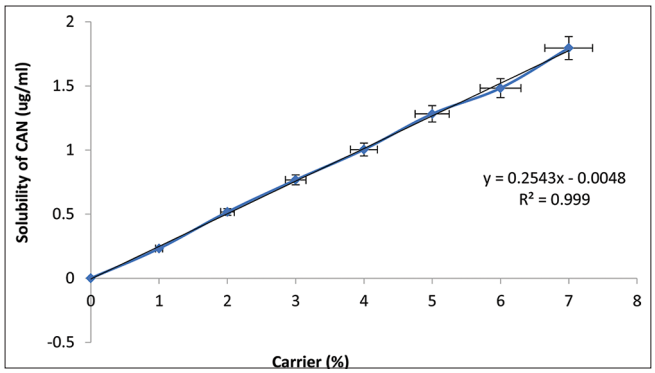

Fig. 5: Phase solubility analysis plot

The comparative solubility study revealed a significant improvement in the aqueous solubility of CC upon nanocrystal and solid dispersion formulation. The pure CC exhibited a solubility of 1.18±0.16 mg/mL, which markedly increased to 2.23±0.12 mg/mL in the nanocrystal form, indicating enhanced dissolution due to particle size reduction and increased surface area. Further enhancement was observed in the nanocrystal-based solid dispersion, which achieved the highest solubility of 2.56±0.10 mg/mL (Fig. 6). This improvement can be attributed to the combined effects of nanosizing, incorporation into a hydrophilic matrix, and the presence of a super-disintegrant, which facilitated better wettability and dispersion. The standard deviation and standard error values also reflect the consistency and reproducibility of the enhanced solubility across formulations [39].

Drug content

CC was synthesized as physical mixes and solid dispersions with PVP-K30 at various drug-to-carrier ratios to conduct preliminary experiments. Based on the findings, it was determined that the drug-polymer ratio of 1:2 gave the best solubility; therefore, this ratio was investigated further. The kneading approach yielded the greatest drug content (92.40%) among the physical combinations and solid dispersions, which varied from 81.12±0.64 to 98.91±1.66 [40].

Dissolution study

CC-loaded solid dispersion with an optimized formulation achieved a 99% drug release at 60 min. The drug release rate was very high in the early intervals. Fig. 7 illustrates how the solid dispersion outperformed the solution in terms of drug release [41].

Drug release kinetics study

Applying the controlled in vitro dissolution results to log the cumulative percentage of drug release versus log time, the KP model produced the

Table 11: Stability study of Optimized batch of nanocrystal formulation (CCNS-9)

Months	Room Temperature (4±2°C)		
	Particle size (nm)	Zeta potential (mv)	Entrapment efficiency (%)
0	221.20±1.32	13.2	92.91±1.23
1	217.38±2.11	13.1	92.65±1.73
2	228.77±1.97	13.6	91.23±1.65
3	222.5±2.45	13.5	91.55±2.98

All values are expressed as mean±standard deviation, n=3

Table 12: Gibbs free energy of transfer for the solubilization process of candesartan cilexetil in aqueous solutions of PVP K–30 at 37°C

Polymer concentration (%w/v)	DGo (kJ/mole)
0.2	0.232±1.123
0.4	0.517±0.548
0.6	0.767±1.65
0.8	1.004±2.78
1	1.282±0.87
1.2	1.483±1.985
1.4	1.796±0.547

All values are expressed as mean±standard deviation, n=3

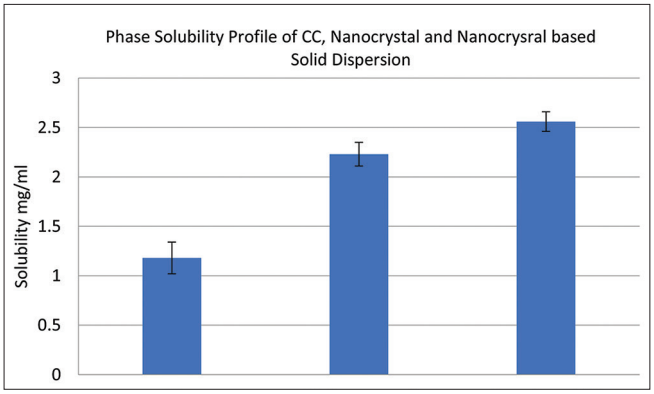

Fig. 6: Comparative solubility study

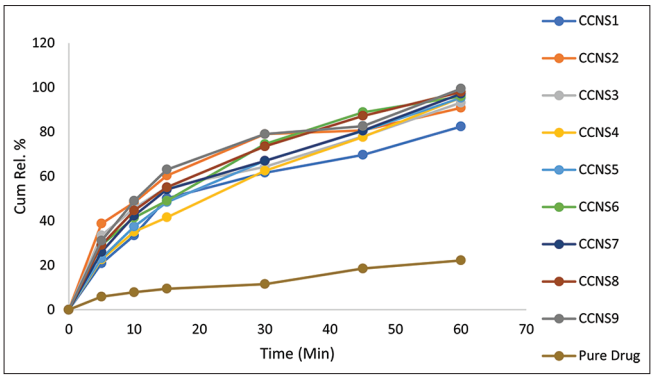

Fig. 7: Comparative drug release profile of all batches of solid dispersion

slopes and R^2 values as shown in Table 13. The *in vitro* release kinetics of the CC-loaded solid dispersion were investigated [42-44]. The regression coefficient (r2) using different kinetic equations is displayed in the table for each batch of solid dispersion. The quantitative analysis of data revealed that the KP model provided the greatest fit for *in vitro* release from solid dispersion. Release exponent, "n," varied from 0.655 to 0.850 and was constructed using the slopes of this model. These values all seem to be in the range of 0.43–0.85, suggesting the formulations have Fickian release kinetics (Fig. 8). This suggests that the solid dispersion with CC intended for topical treatment follows a Fickian diffusion mechanism. Using this method resulted in a more uniform dispersion of CC, as the *in vitro* investigations showed (Table 13) [43].

TEM study of solid dispersion powder

TEM pictures produced by the lyophilization process of a CCNS-9 the TEM pictures demonstrate a smooth and spherical structure of the solid dispersion, indicating some degree of particle stabilization. This feature suggests that the dispersion of solids might not cause discomfort. When defined as a monodisperse distribution of nanoparticles, solid dispersions usually show a limited range of particle sizes (Fig. 9) [45,46].

***In vivo* pharmacokinetics study of CC nanocrystal-loaded solid dispersion**

This study included a topically administered comparison with a commercially available CC formulation. After 6.12 min of retention, the chromatographic analysis showed a single peak that was identified as CC. The plasma concentrations of candesartan were determined at different times using the HPLC technique [47].

AUC, C_{max}, and T_{max} were among the parameters that were assessed on blood samples that were taken from each of the three groups. Table 11 shows that the C_{max} values were ascertained: CC optimized formulation yielded 3.457±19.36, its marketed formulation produced

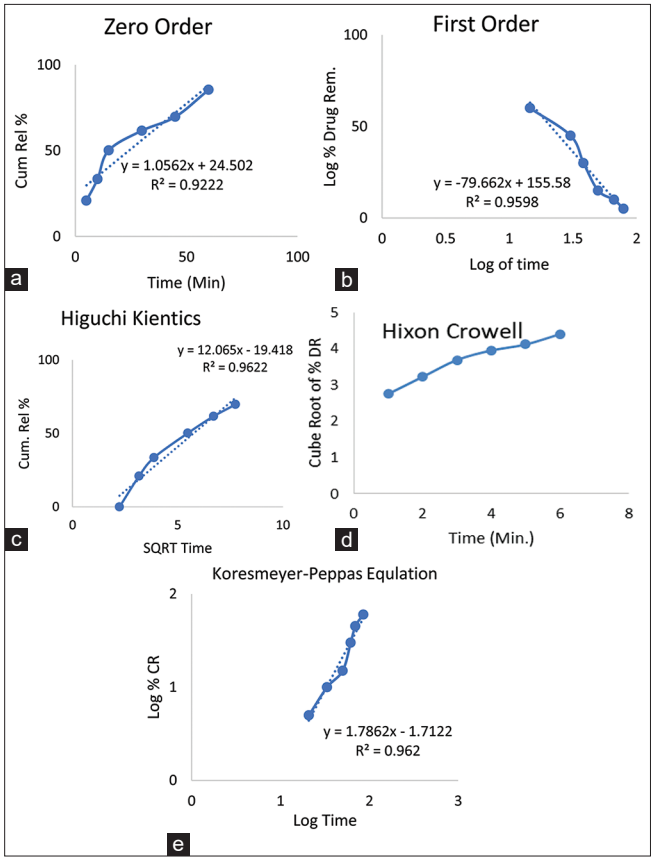

Fig. 8: *In vitro* release kinetics profile of (a) Zero order (b) First order (c) Higuchi Kinetics (d) Hixon Crowell model (e) Korsemeyer-Peppas Equation

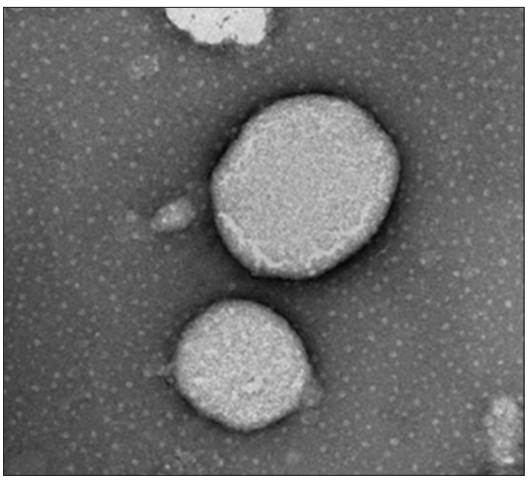

Fig. 9: Transmission electron microscopy of candesartan cilexetil loaded solid dispersion

6.985±2.456, and CC-based nanocrystalline solid dispersion produced 20.789±0.6549. According to the findings, the corresponding T_{max} are 4±0.2567 min., 5±0.246 min., and 6±0.45 min. 6987.78±21.98 µg/mL.h for CC-based nanocrystalline solid dispersion, 4178.69±18 µg/mL.h for the marketed formulation of CC, and 3825.98±39.85 µg/mL.h for the optimized formulation of nanocrystal were the results obtained in terms of AUC [48,49]. Two components were used to conduct the pharmacokinetic investigation, and the findings are as well as Table 11 summary of the outcomes. It is clear from the results that T_{max}, C_{max}, and AUC all peaked with the optimized CC formulation. Significantly, the C_{max} exhibited by the Plane nanosuspension of CC was 5 times

Table 13: Kinetic profiles of *in vitro* drug release of solid dispersion

Formulation Code	R^2			Korsemeyer-Pappas Equation	
	Zero Order	First Order	Higuchi Kinetics	R^2	n (slope)
CCSD-1	0.9739	0.9564	0.9356	0.8729	0.4572
CCSD-2	0.9898	0.9522	0.9564	0.887	0.4251
CCSD-3	0.9944	0.9598	0.9666	0.9085	0.4284
CCSD-4	0.9987	0.9897	0.9598	0.8863	0.4363
CCSD-5	0.9812	0.9978	0.9698	0.8828	0.4469
CCSD-6	0.9897	0.9987	0.9789	0.933	0.4535
CCSD-7	0.9822	0.9632	0.9898	0.9468	0.4785
CCSD-8	0.9798	0.9978	0.9987	0.9551	0.4613
CCSD-9	0.9932	0.9878	0.9899	0.9253	0.4374

Table 14: Results of *in vivo* pharmacokinetics study

Parameters	Candesartan cilexetil nanocrystal	Candesartan cilexetil-based nanocrystalline solid dispersion	Marketed formulation of candesartan cilexetil
AUC (µg/mL.h)	3825.98±39.85	6987.78±21.98	4178.69±18
C_{max} (µg/mL)	3.457±19.36	20.789±0.6549	6.985±2.456
T_{max} (min.)	4±0.2567	6±0.45	5±0.246

All values are expressed as mean±standard deviation, n=3. AUC: Area under the curve

higher than that of the optimized formulation and double that of the marketed formulation. Moreover, the increased bioavailability of the CC formulation was indicated by the AUC, which was higher for the optimized formulation than for the other formulation. Table 14 shows the results of *in vivo* pharmacokinetics study.

CONCLUSION

Enhancing drug absorption through improved permeability, dissolution, and solubility remains a key focus in pharmaceutical development. Poor aqueous solubility often leads to *in vivo* challenges such as low bioavailability, food-dependent absorption, inter-patient variability, and incomplete drug release from the dosage form. CC, a lipophilic compound with limited water solubility and a known P-glycoprotein substrate, exemplifies these limitations. To address this, high-energy amorphous systems such as lyophilized solid dispersions have shown promise. These systems enhance solubility through disruption of the drug's crystalline structure and the solubilizing effect of hydrophilic carriers. The current study supports the potential of such solid dispersion strategies to significantly improve the aqueous solubility and, consequently, the bioavailability of poorly soluble drugs like CC.

ACKNOWLEDGMENTS

The authors would like to extend their sincere gratitude to the Government College of Pharmacy, Karad, Satara, Maharashtra, India, for providing excellent research infrastructure for the completion of the present investigation.

AUTHORS' CONTRIBUTIONS

All authors have contributed to the conception and design of the study. The original manuscript draft was authored by Sonali Vijaykumar Magdum, with subsequent input and revisions provided by all authors on prior iterations of the manuscript. All study designs, all kinds of data interpretation, and guidance for MS text preparation were directed by Pramodkumar J. Shirote. All authors have thoroughly reviewed and endorsed the final version of the manuscript.

CONFLICT OF INTEREST STATEMENT

The Authors declared no conflict of interest

REFERENCES

1. Aly UF, Sarhan HA, Monsef Ali TF, Sharkawy HA. Applying different techniques to improve the bioavailability of candesartan cilexetil antihypertensive drug. Drug Des Devel Ther. 2020;14:1851-65. doi: 10.2147/DDDT.S248511
2. Al-Edresi S, Hamrah KA, Al-Shaibani A. Formulation and validation of candesartan cilexetil-loaded nanosuspension to enhance solubility. J Pharm. 2024;71:1-13. doi: 10.3897/pharmacia.71.e114943
3. Poudel S, Kim DW. Developing pH-modulated spray dried amorphous solid dispersion of candesartan cilexetil with enhanced *in vitro* and *in vivo* performance. Pharmaceutics. 2021;13(4):497. doi: 10.3390/pharmaceutics13040497
4. Dudhipala N, Veerabrahma K. Candesartan cilexetil loaded solid lipid nanoparticles for oral delivery: Characterization, pharmacokinetic and pharmacodynamic evaluation. Drug Deliv. 2016;23(2):395-404. doi: 10.3109/10717544.2014.914986
5. Phalak SD, Bodke VI, Yadav RE, Pandav SA, Ranaware MA. A systematic review on nano drug delivery system: Solid lipid nanoparticles (SLN). Int J Curr Pharm Res. 2024;16(1):10-20. doi: 10.22159/ijcpr.2024v16i1.4020
6. Bhairav BA, Jagtap LR, Saudagar RB. Solubility and dissolution enhancement of Pioglitazone using solid dispersion technique. Int J Curr Pharm Res. 2017;9(5):186-93. doi: 10.22159/ijcpr.2017v9i5.22326
7. Gauniya AN, Mazumder RU, Pathak KA. Formulation, optimization and characterization of ziprasidone nanocrystals prepared by media milling technique. Int J Pharm Pharm Sci. 2015;7:146-50.
8. Surampalli G, Nanjwade BK, Patil PA, Chilla R. Novel tablet formulation of amorphous candesartan cilexetil solid dispersions involving P-gp inhibition for optimal drug delivery: *In vitro* and *in vivo* evaluation. Drug Deliv. 2016;23(7):2124-38. doi: 10.3109/10717544.2014.945017
9. Kamble SS, Gambhire MS, Gujar KN. Optimization and development of candesartan cilexetil loaded solid lipid nanoparticle for the treatment of hypertension. J Pharm Biosci. 2015;3:53-64.
10. Albaidhani SF, Hussein AA. Preparation and evaluation of solid supersaturable self-nanoemulsifying drug delivery system of candesartan cilexetil. J Pharm Sci Res. 2019;11(3):859-68.
11. Diwan R, Ravi PR, Pathare NS, Aggarwal V. Pharmacodynamic, pharmacokinetic and physical characterization of cilnidipine loaded solid lipid nanoparticles for oral delivery optimized using the principles of design of experiments. Colloids Surf B Biointerfaces. 2020;193:111073. doi: 10.1016/j.colsurfb.2020.111073
12. AboulFotouh K, Allam AA, El-Badry M, El-Sayed AM. Development and *in vitro*/*in vivo* performance of self-nanoemulsifying drug delivery systems loaded with candesartan cilexetil. Eur J Pharm Sci. 2017;109:503-13. doi: 10.1016/j.ejps.2017.09.001
13. Guan H, Wang M, Yu S, Wang C, Chen Q, Chen Y, *et al*. Candesartan cilexetil formulations in mesoporous silica: Preparation, enhanced dissolution *in vitro*, and oral bioavailability *in vivo*. J Pharm Sci. 2024;113(10):3045-53. doi: 10.1016/j.xphs.2024.07.007
14. Lokeshvar R, Ramaiyan V, Nithin V, Pavani S, Vinod Kumar T. Nanotechnology-driven therapeutics for liver cancer: Clinical applications and pharmaceutical insights. Asian J Pharm Clin Res. 2025;18(2):8-26. doi: 10.22159/ajpcr.2025v18i2.53429
15. Bisht T, Bolmal UB, Nainwal N. Formulation of candesartan cilexetil nanoparticles by ionotropic gelation method using ultrasonication. Indian J Pharm Educ Res. 2023;57(3):728-35.
16. Khanfar M, Al Taani BA, Mohammad E. Enhancement of dissolution and stability of candesartan cilexetil-loaded silica polymers. Int J Appl Pharm. 2019;11(2):64-70. doi: 10.22159/ijap.2019v11i2.30411
17. Fouad AG, Ali MR, Naguib DM, Farouk HO, Zanaty MI, El-Ela FI. Design, optimization, and *in vivo* evaluation of invasome-mediated candesartan for the control of diabetes-associated atherosclerosis. Drug Deliv Transl Res. 2024;14(2):474-90. doi: 10.3390/ph18010031
18. Yiyan MO, Jingmeng SU, Chenchen FA, Zhenzhen JI, Xin ZH, Weiyu ZH. Construction and characterization of candesartan cilexetil P123/F127 mixed micelle delivery system. Herald Med. 2022;41(12):1828-35. doi: 10.1080/03639045.2023.2293122
19. Mady OY, Abulmeaty MM, Donia AA, Al-Khureif AA, Al-Shoubki AA, Abudawood M, *et al*. Formulation and bioavailability of novel mucoadhesive buccal films for candesartan cilexetil in rats. Membranes. 2021;11(9):659. doi: 10.3390/membranes11090659
20. Awadeen RH, Boughdady MF, Meshali MM. Quality by design

approach for preparation of zolmitriptan/chitosan nanostructured lipid carrier particles-formulation and pharmacodynamic assessment. Int J Nanomedicine. 2020;15:8553-68. doi: 10.2147/IJN.S274352

21. Jain S, Patel K, Arora S, Reddy VA, Dora CP. Formulation, optimization, and *in vitro-in vivo* evaluation of olmesartan medoxomil nanocrystals. Drug Deliv Transl Res. 2017;7(2):292-303. doi: 10.1007/s13346-016-0355-2
22. Zafar A, Alruwaili NK, Imam SS, Alsaidan OA, Alharbi KS, Yasir M, *et al*. Formulation of chitosan-coated piperine NLCs: Optimization, *in vitro* characterization, and *in vivo* preclinical assessment. AAPS PharmSciTech. 2021;22(7):231. doi: 10.1208/s12249-021-02098-4
23. Yuksel N, Bayindir ZS, Aksakal E, Ozcelikay AT. *In situ* niosome forming maltodextrin proniosomes of candesartan cilexetil: *In vitro* and *in vivo* evaluations. Int J Biol Macromol. 2016;82:453-63. doi: 10.1016/j.ijbiomac.2015.10.019
24. Harish V, Tewari D, Mohd S, Govindaiah P, Babu MR, Kumar R, *et al*. Quality by design-based formulation of xanthohumol loaded solid lipid nanoparticles with improved bioavailability and anticancer effect against PC-3 cells. Pharmaceutics. 2022;14(11):2403. doi: 10.3390/pharmaceutics14112403
25. Madan JR, Patil K, Awasthi R, Dua K. Formulation and evaluation of solid self-microemulsifying drug delivery system for azilsartan medoxomil. Int J Polym Mater Polym Biomater. 2021;70(2):100-16. doi: 10.1080/00914037.2019.1695206
26. Sharma S, Sharma JB, Bhatt S, Kumar M. Optimization and fabrication of curcumin loaded solid lipid nanoparticles using box-Behnken design for nasal delivery. Nanosci Nanotechnol Asia. 2022;12(6):7-18. doi: 10.2174/2210681213666221103151333
27. El-Housiny S, Fouad AG, El-Bakry R, Zaki RM, Afzal O, El-Ela FI, *et al*. *In vitro* and *in vivo* characterization of nasal pH-responsive *in-situ* hydrogel of candesartan-loaded invasomes as a potential stroke treatment. Drug Deliv Transl Res. 2024;15:1626-45.doi: 10.1007/s13346-024-01700-z
28. Abla KK, Mneimneh AT, Allam AN, Mehanna MM. Application of Box-Behnken design in the preparation, optimization, and *in-vivo* pharmacokinetic evaluation of oral tadalafil-loaded niosomal film. Pharmaceutics. 2023;15(1):173. doi: 10.3390/pharmaceutics15010173
29. Reddy KT, Dharmamoorthy G, Vasavi Devi D, Vidiyala N, Bagade OM, Elumalai S, *et al*. Phytoconstituent based green synthesis of nanoparticles: Sources and biomedical applications in cancer therapy. Asian J. Green Chem. 2025;9(3):329-54. doi: 10.48309/ajgc.2025.501113.1669
30. Jain S, Reddy VA, Arora S, Patel K. Development of surface stabilized candesartan cilexetil nanocrystals with enhanced dissolution rate, permeation rate across CaCo-2, and oral bioavailability. Drug Deliv Transl Res. 2016;6(5):498-510. doi: 10.1007/s13346-016-0297-8
31. Detroja C, Chavhan S, Sawant K. Enhanced antihypertensive activity of candesartan cilexetil nanosuspension: Formulation, characterization and pharmacodynamic study. Scientia pharmaceutica. 2011;79(3):635-52. DOI: 10.3797/scipharm.1103-17.
32. Amer AM, Allam AN, Abdallah OY. Preparation, characterization and *ex vivo-in vivo* assessment of candesartan cilexetil nanocrystals via solid dispersion technique using an alkaline esterase activator carrier. Drug Dev Ind Pharm. 2019;45(7):1140-8. doi: 10.1080/03639045.2019.1600533
33. Anwar W, Dawaba HM, Afouna MI, Samy AM. Screening study for formulation variables in preparation and characterization of candesartan cilexetil loaded nanostructured lipid carriers. Univ J Pharm Res. 2019;4(6):1-24.
34. Sharma M, Singh B. Formulation and evaluation of self-emulsifying drug delivery systems for candesartan cilexetil. Int J Pharm Sci Nanotechnol. 2022;15(2):5844-54. doi: 10.37285/ijpsn.2022.15.2.3
35. Zewail MB, El-Gizawy SA, Osman MA, Haggag YA. Preparation and *in vitro* characterization of a novel self-nano emulsifying drug delivery system for a fixed-dose combination of candesartan cilexetil and hydrochlorothiazide. J Drug Deliv Sci Technol. 2021;61:102320. doi: 10.1016/j.jddst.2021.102320
36. Ali IS, Sajad UA, Abdul Rasool BK. Solid dispersion systems for enhanced dissolution of poorly water-soluble candesartan cilexetil: *In vitro* evaluation and simulated pharmacokinetics studies. PLoS One. 2024;19(6):e0303900.
37. Nekkanti V, Karatgi P, Prabhu R, Pillai R. Solid self-microemulsifying formulation for candesartan cilexetil. Aaps Pharmscitech. 2010;11:9-17. doi: 10.1208/s12249-009-9347-6.
38. Sezgin-Bayindir Z, Antep MN, Yuksel N. Development and characterization of mixed niosomes for oral delivery using candesartan cilexetil as a model poorly water-soluble drug. AAPS pharmscitech. 2015;16:108-17. doi: 10.1208/s12249-014-0213-9.
39. Ali HH, Hussein AA. Oral nanoemulsions of candesartan cilexetil: Formulation, characterization and *in vitro* drug release studies. AAPS Open. 2017;3(4):4.
40. Devi AS, Pinnika A, Divya P. Formulation and evaluation of candesartan cilexetil transdermal proniosomal gel. J Drug Deliv Ther. 2014;4(2):90-8. doi: 10.22270/jddt.v4i2.813
41. Mauludin R, Müller RH, Keck CM. Development of an oral rutin nanocrystal formulation. Int J Pharm. 2009;370(1-2):202-9. doi: 10.1016/j.ijpharm.2008.11.029
42. Ige PP, Baria RK, Gattani SG. Fabrication of fenofibrate nanocrystals by probe sonication method for enhancement of dissolution rate and oral bioavailability. Colloids Surf B Biointerfaces. 2013;108:366-73. doi: 10.1016/j.colsurfb.2013.02.043
43. Sharma OP, Patel V, Mehta T. Design of experiment approach in development of febuxostat nanocrystal: Application of soluplus® as stabilizer. Powder Technol. 2016;302:396-405. doi: 10.1016/j.powtec.2016.09.004
44. Qushawy M, Nasr AL. Solid lipid nanoparticles (SLNs) as nano drug delivery carriers: Preparation, characterization and application. Int J App Pharm. 2020;12(1):1-9. doi: 10.22159/ijap.2020v12i1.35312
45. Chaudhari PD, Desai US. Formulation and evaluation of niosomal in situ gel of prednisolone sodium phosphate for ocular drug delivery. Int J App Pharm. 2019;11(2):97-116. doi: 10.22159/ijap.2019v11i2.30667
46. Aparna C, Anusha M, Manisha B. Enhancement of dissolution of candesartan cilexetil. Asian J Pharm Clin Res. 2023;16(3):148-51.
47. Koradia KD, Parikh RH, Koradia HD. Albendazole nanocrystals: Optimization, spectroscopic, thermal and anthelmintic studies. J Drug Deliv Sci Technol. 2018;43:369-78.doi: 10.1016/j.jddst.2017.11.003
48. Vardaka E, Kachrimanis K. Nanocrystal formulations of mebendazole employing quality by design and molecular level insights by atomistic simulations. Drug Dev Ind Pharm. 2024;89:256-301. doi: 10.1080/03639045.2024.2398597
49. Deepthi VV, Swathi N, Gollu G, Nalini M. Cramming on potato starch as a novel super-disintegrant for depiction and characterization of candesartan cilexetil fast dissolving tablet. Thai J Pharm Sci. 2021;45(2):143-7.